Anomalous Low-Temperature Enhancement of Supercurrent in Topological-Insulator Nanoribbon Josephson Junctions: Evidence for Low-Energy Andreev Bound States

Morteza Kayyalha,[1,*] Mehdi Kargarian,[2] Aleksandr Kazakov,[3] Ireneusz Miotkowski,[3] Victor M. Galitski,[2] Victor M. Yakovenko,[2] Leonid P. Rokhinson,[3,1,4] and Yong P. Chen[3,1,4,5,†]

[1]*School of Electrical and Computer Engineering and Birck Nanotechnology Center, Purdue University, West Lafayette, Indiana 47907, USA*

[2]*Department of Physics, Condensed Matter Theory Center and Joint Quantum Institute, University of Maryland, College Park, Maryland 20742, USA*

[3]*Department of Physics and Astronomy, Purdue University, West Lafayette, Indiana 47907, USA*

[4]*Purdue Quantum Center, Purdue University, West Lafayette, Indiana 47907, USA*

[5]*WPI-AIMR International Research Center on Materials Sciences, Tohoku University, Sendai 980-8577, Japan*

(Received 29 November 2017; revised manuscript received 9 October 2018; published 1 February 2019)

We report anomalous enhancement of the critical current at low temperatures in gate-tunable Josephson junctions made from topological insulator $BiSbTeSe_2$ nanoribbons with superconducting Nb electrodes. In contrast to conventional junctions, as a function of the decreasing temperature T, the increasing critical current I_c exhibits a sharp upturn at a temperature T_* around 20% of the junction critical temperature for several different samples and various gate voltages. The I_c vs T demonstrates a short junction behavior for $T > T_*$, but crosses over to a long junction behavior for $T < T_*$ with an exponential T dependence $I_c \propto \exp(-k_B T/\delta)$, where k_B is the Boltzmann constant. The extracted characteristic energy scale δ is found to be an order of magnitude smaller than the induced superconducting gap of the junction. We attribute the long-junction behavior with such a small δ to low-energy Andreev bound states arising from winding of the electronic wave function around the circumference of the topological insulator nanoribbon.

DOI: 10.1103/PhysRevLett.122.047003

Three-dimensional (3D) topological insulators (TI) are characterized by insulating bulk and nontrivial conducting surface states, where the spin is helically locked perpendicular to the momentum, and the carriers are massless Dirac fermions with linear energy-momentum dispersion [1–3]. Theoretical work by Fu and Kane [4] has predicted that, once coupled to an s-wave superconductor, the surface states of TIs can undergo unconventional superconducting pairing, which can provide a useful platform to study exotic phenomena such as topological superconductivity and Majorana fermions [2,4]. In contrast to the conventional spin-singlet superconductivity, the induced superconductivity in the surface states of a 3D TI [4] is a mixture of singlet and triplet pairings due to the lifted spin degeneracy [5–7]. Furthermore, Andreev bound states (ABS) formed within a superconductor-TI-superconductor (S-TI-S) Josephson junction (JJ) can exhibit a robust zero-energy crossing when the phase difference between the two superconductors is π, giving rise to Majorana modes [4,6]. Possible probes of topological superconductors or junctions may include the tunneling spectroscopy, the current-phase relation (CPR), and temperature dependence of the critical current [8–13].

In recent years, S-TI-S JJs with two- and three-dimensional TIs have been extensively studied. Gate-tunable supercurrent and Josephson effects have also been observed [14–29]. However, in many of the devices studied so far, the bulk of the TI can have notable contributions to the transport properties of the junction and make it difficult to separate out the contribution of the surface states.

In this work, we use the topological insulator $BiSbTeSe_2$ with a distinct advantage that at low temperatures the bulk is insulating and only the surface states contribute to electrical transport [29–31]. We obtain nanoribbons of $BiSbTeSe_2$ using the exfoliation technique and fabricate superconductor-(TI nanoribbon)-superconductor (S-TINR-S) JJs. Because of the enhanced surface to volume ratio, uniform cross-sectional area, and relatively small size, TINR-based devices are an excellent platform to study topological transport, exhibiting ballistic conduction and π-Berry-phase Aharonov-Bohm effects [32–34], and are also predicted to be promising for study of topological superconductivity [35,36]. In our TINR-based JJs, in contrast to conventional junctions, we observe a sharp upturn of the critical current I_c for temperatures T below ~20% of the junction critical temperature T_c. Interestingly, this upturn temperature ($\sim 0.2T_c$) is observed in a variety of JJs with different gate voltages V_g's. We interpret the experimental results using a phenomenological model for junctions based on TINRs. This model relates the enhancement of

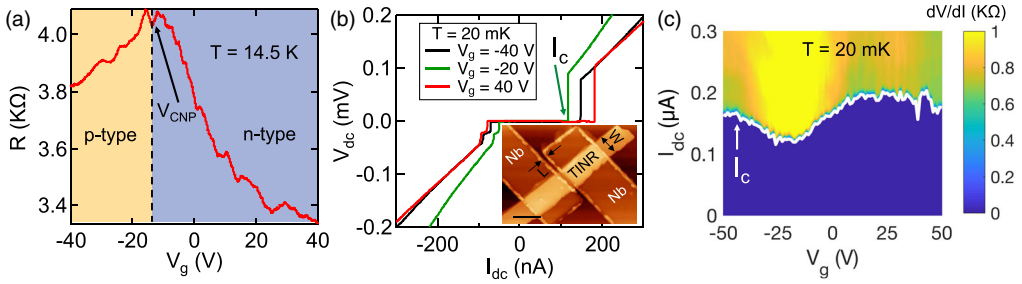

FIG. 1. (a) Two-terminal R vs V_g measured at $T = 14.5$ K, above the critical temperature $T_c^{\mathrm{Nb}} = 7.5$ K of the Nb electrodes. Shaded regions highlight n and p doping of TINR. (b) V_{dc} vs I_{dc} for different V_g's at $T = 20$ mK. Inset: AFM image of sample 1 (from which all data in this figure are measured), a TI ($BiSbTeSe_2$) nanoribbon Josephson device with superconducting Nb electrodes. Scale bar is 0.5 μm. (c) Color map of the two-terminal dV/dI vs V_g and I_{dc} at $T = 20$ mK. An ac excitation current $I_{\mathrm{ac}} = 1$ nA was used for the dV/dI measurement. Solid white line marks the junction critical current I_c vs V_g. Data in (b)–(c) is measured by sweeping I_{dc} from -300 to 300 nA.

I_c at low temperatures to the ABS whose energy scale is around an order of magnitude smaller than the induced superconducting gap. The reduced energy scale of the ABS is attributed to the winding of their wave function around the circumference of the TINR. Such ABS are in the long junction limit and give rise to an exponential enhancement of I_c with decreasing T. Furthermore, we observe a sinusoidal current-phase relation measured using an asymmetric superconducting quantum interference device (SQUID), consistent with the expectation for these samples at our measurement temperature.

We study a variety of TINR JJs with niobium (Nb) as the superconductor, details regarding device fabrication and sample parameters can be found in the Supplemental Material [37]. We have previously observed large I_cR_N product (where R_N is the normal-state resistance) and multiple Andreev reflections in such TINR JJs [29], demonstrating the high quality of the junctions including the Nb-TINR interface. Inset of Fig. 1(b) depicts an atomic force microscope (AFM) image of a representative S-TINR-S junction (sample 1).

Figure 1(a) shows the ambipolar field effect in the two-terminal resistance R vs V_g measured in sample 1 at $T = 14.5$ K, above T_c of Nb. By varying V_g, the carrier type in the TINR can be changed from n type to p type, and the chemical potential can be tuned into the bulk band gap to be in the TSS. The gate voltage where the maximum of R vs V_g occurs represents the charge neutrality point (CNP) which is $V_{\mathrm{CNP}} \sim -15$ V for this sample.

The junction $T_c \sim 0.5$–2.2 K, the temperature below which the junction resistance vanishes, is much lower than the T_c of Nb ($T_c^{\mathrm{Nb}} \sim 7.5$ K) in our JJs. The dc voltage V_{dc} vs the dc current I_{dc}, measured in sample 1 when sweeping I_{dc} from -300 to 300 nA at $T = 20$ mK for a few different V_g's is plotted in Fig. 1(b). When I_{dc} is small, the voltage across the junction is zero, indicating that the junction is in its superconducting state and supports a supercurrent (I_{dc}). However, once the current is increased above some critical current (defined as I_c, marked by the arrow for the $V_g = -20$ V curve), the junction leaves the superconducting state and transitions to the normal state with a finite voltage drop. Figure 1(c) shows the color map of the two-terminal differential resistance dV/dI vs V_g and I_{dc} (swept from 0 to 300 nA) at $T = 20$ mK. The solid white line in this figure marks the critical current I_c of the junction. Notably, we observe that I_c exhibits an ambipolar field effect (which has not been realized in previous devices [22,23,29]) and reaches a minimum of $\sim$120 nA near $V_{\mathrm{CNP}} \sim -15$ V, consistent with the peak in R vs V_g measurement [Fig. 1(a)].

Figure 2(a) shows the T dependence of I_c for three different V_g's in sample 1. Starting from T_c, I_c increases with decreasing T. Notably, we observe an anomaly in I_c vs T at an upturn temperature ($T_* \sim 0.36$ K marked for the $V_g = 45$ V dataset with $T_c \sim 2.2$ K as an example), below which I_c increases sharply and eventually reaches its largest value I_c^{max} at the lowest accessible temperature ($T \sim 20$ mK). The normalized I_c/I_c^{max} vs the normalized T/T_c for this sample is depicted in Fig. 2(b). Interestingly, T_* is always $\sim 0.2T_c$ for this sample regardless of V_g. Figure 2(c) plots I_c/I_c^{max} vs T/T_c for five different samples, with each sample measured at a few V_g's. We observe that T_*/T_c remains $\sim$0.2 for all our TINR-based JJs, regardless of their T_c and V_g (see Table S1 in the Supplemental Material [37]). Noteworthy, we observe an exponential enhancement of I_c with decreasing T for $T < T_*$ as highlighted by the solid red lines in Figs. 2(b) and 2(c).

The anomalous temperature dependence of I_c observed in our samples is radically different from that of conventional JJs. While the T dependence of our I_c for $T_* < T < T_c$ maybe described by the behavior of a TI-based *short* junction [e.g., solid blue line in Fig. 2(b), as discussed more in our model presented below], I_c of such short junctions is *not* expected to exhibit any exponential behavior before it saturates at low temperatures [6,10]. However, for *long* junctions, I_c increases exponentially with decreasing temperature [38–42] before its eventual saturation at the low temperature limit. Therefore, the increase in I_c vs decreasing T for $T_* < T < T_c$ followed by an exponential

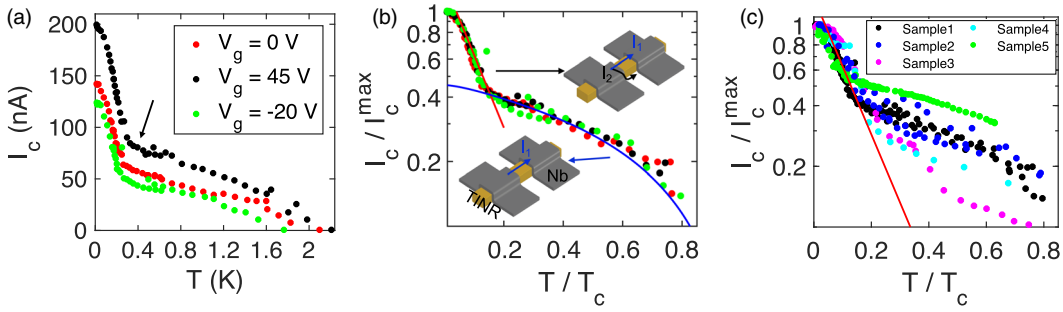

FIG. 2. (a) Temperature dependence of I_c for different V_g's for sample 1. (b) Normalized $I_c/I_c^{\max}$ vs normalized T/T_c for data in (a) in log-linear scale. The solid blue line is the normalized $I_{c1}/I_{c1}^{\max}$ [Eq. (2)] divided by factor 2.2 and the solid red line is a fit to $\exp(-k_BT/\delta)$ with $\delta \sim 0.08\Delta$. The symbols have the same legends as in (a). Inset: cartoons of the TINR JJ depicting the current I_1 corresponding to the modes on the top surface and the current I_2 corresponding to the modes that extend around the circumference and flow through the bottom surface. (c) $I_c/I_c^{\max}$ vs T/T_c in a log-linear scale for five different TINR-based Josephson devices measured at a few (1–3) V_g's for each device. The exponential fit and the experimental data in (b) are also included in this plot as the solid red line and black symbols, respectively.

enhancement of I_c for $T < T_*$ as observed in Fig. 2(b) suggests that I_c in our samples may be dominated by a short junction behavior for $T > T_*$ and a long junction behavior for $T < T_*$. Such a transition from short to long junction behaviors may be related to the nature of the TSS in the TINR. Because, the TSS extend over the entire circumference of the TINR, the superconducting transport is carried by modes on both the top [corresponding to I_1 depicted in the inset of Fig. 2(b)] and bottom [corresponding to I_2 depicted in the inset of Fig. 2(b)] surfaces of the TINR, i.e., the total supercurrent $I = I_1 + I_2$.

For the TINR with a circumference $C = 2W + 2t$, the transverse momentum k_y, perpendicular to the current, is quantized as $k_y = (2\pi/C)(n + 1/2)$, where n is an integer [43,44]. Also note in our TINR the current flows between the superconducting contacts fabricated on the top surface. Therefore, the modes with $k_y \sim 0$ remain on the top surface and contribute to I_1, while the modes with $|k_y| \gg 0$ extend around the perimeter of the TINR and contribute to I_2. We note that the $k_y = 0$ mode is prohibited in the TINR.

The modes (corresponding to I_1) on the top surface travel a short distance L, the separation between the two Nb contacts, and are supposedly in the short-junction limit. We found our experimental data of I_c vs T for $T > T_*$ can be described using the temperature-dependent supercurrent calculated for a ballistic short junction [6,10,39], given by

$$I_1(\phi, T) = N_1 \frac{e\pi\Delta(T)}{h} \sin\left(\frac{\phi}{2}\right) \tanh\left(\frac{\Delta(T)\cos(\frac{\phi}{2})}{2k_BT}\right), \quad (1)$$

where h is the Plank constant, k_B is the Boltzmann constant, e is the electron charge, N_1 is the number of modes in the top surface, ϕ is the phase difference between the two superconductors, and $\Delta(T)$ is the induced superconducting gap. We assume a BCS temperature dependence for $\Delta(T)$ with $\Delta(T=0) = \Delta_0 = 1.76k_BT_c$ [45].

We obtain the critical current $I_{c1}(T)$ by maximizing $I_1(\phi, T)$ over ϕ as

$$I_{c1}(T) = \max_{\phi}(I_1(\phi, T)). \quad (2)$$

We have plotted $I_{c1}(T)$ calculated from Eq. (2) to obtain the solid blue curve in Fig. 2(b). The computed $I_{c1}(T)/I_{c1}^{\max}$, where $I_{c1}^{\max} = I_{c1}(T = 0)$, is divided by 2.2 in order to show its agreement with experimental results for $T > T_*$ in the normalized version of $I_c/I_c^{\max}$ in Fig. 2(b) (this indicates I_{c1} on the top surface contributes nearly half of the total I_c at the low temperature limit).

In contrast, the modes (corresponding to I_2) flowing through the bottom surface extend over the entire circumference [$C \sim 700$ nm for sample 1 shown in Figs. 2(a) and 2(b)] of the TINR (through the side surface) and hence travel a longer distance d ($d \geq C \gg L$, with $L = 40$ nm for sample 1). We assume such modes are in the ballistic long-junction limit with $d \geq \xi$, where $\xi = \hbar v_F/\Delta \sim 640$ nm is the superconducting coherence length of the junction and $v_F = 3 \times 10^5$ m/s is the Fermi velocity. As a result, we observe a reduced energy gap $\delta = \hbar v_F/2\pi d$ for these modes [39,42,46–48]. In the limit of $T_{\rm sat} < T < T_*$, where $T_{\rm sat} \ll \delta/k_B$ is the temperature below which I_c saturates, the critical current of these modes exhibits an exponential dependence on T, i.e., $I_c \propto \exp(-k_BT/\delta)$ [39,42,46–48]. This exponential dependence is seen in the experimental data in Fig. 2(b). To extract δ, we perform an exponential fit to I_c for $T_{\rm sat} < T < T_*$ (where we take $T_{\rm sat} \sim 0.04T_c$) as depicted by the solid red line in Fig. 2(b). The fit gives $\delta \sim 0.08\Delta$, corresponding to $d = (\hbar v_F/2\pi\delta) \sim 1.2$ μm, which is quite close to $\sim\xi + C$. We have found similar trends for the extracted $d \sim C + \xi$ in other samples shown in Fig. 2(c) (see also Fig. S2d in the Supplemental Material [37]). We suggest that when the effective length d is on the order of ξ, the extracted δ should be proportional to

$1/(C+\xi)$ rather than $1/C$ (thus d should be closer to $C+\xi$ rather than C). This reduced δ is also consistent with the discussions in Ref. [42]. To highlight the influence of ξ on δ (and T_*), we have plotted δ and T_* vs $1/(C+\xi)$ in Fig. S2b [37]. Consistent with our expectation, we observe that δ (and T_*) increases with increasing $1/(C+\xi)$.

We can extract $N_1 \sim 1$–5 for different samples from the fit of I_{c1} as determined by Eq. (2) to the experimental results. The extracted value of N_1 is much smaller than the estimated total number of modes $N = k_F C/2\pi \sim 24$–114, where $k_F = \sqrt{4\pi(C_g/e)(V_g - V_{\mathrm{CNP}})}$ is the Fermi wave vector and $C_g = 12$ nF/cm^2 is the parallel plate capacitance per unit area of a 300-nm SiO_2 [37]. Furthermore, we can estimate the number of modes N_2 corresponding to I_2 as $N_2 = N - N_1 \sim (10$–$20)N_1$. This suggests that the majority of the modes in our TINRs are going around the circumference and through the bottom surface to contribute to I_2, consistent with the expectation that only modes with k_y near zero contribute to I_1. We note that I_c at the lowest T is proportional to the number of modes and the energy scale of the ABS in both the long and short junction limits (i.e., the low-T I_1 and I_2 are proportional to $N_1\Delta_0$ and $N_2\delta$, respectively). The extracted large $N_2 \sim (10$–$20)N_1$ and the small $\delta \sim 0.1\Delta_0$ imply that the contribution of I_1 and I_2 to the total critical current at low T should be comparable, which is consistent with our experimental observations in Figs. 2(b) and 2(c). For instance, I_{c1} represented by the solid blue line in Fig. 2(b) approaches ~50% of the total I_c when extrapolated to the lowest T.

In the above phenomenological model, we have used one effective reduced gap δ to describe all the modes flowing around the circumference and through the bottom surface. However, in reality these modes can have different gaps depending on how far they travel between the two superconductors. Currently there is no theory for the temperature dependence of I_c specific to TINR (considering the wrapping of the electronic wave function around the circumference). Further studies are required to fully understand the nature of the induced superconductivity in this system.

We have measured the CPR (supercurrent I vs phase ϕ) in our TINR junction at $T = 20$ mK using an asymmetric SQUID based on our TINR junction in parallel with a reference junction [37,49,50]. Figure 3(a) depicts a scanning electron microscope (SEM) image of the SQUID. The measured CPR (symbols) is shown in Fig. 3(b) alongside a sinusoidal function (black curve), which describes well the measured CPR.

It has been predicted that in a TI flake, regardless of the barrier height Z imposed by a nonmagnetic impurity, $k_y = 0$ mode will have a transmission probability $D = 1$ and will give rise to a highly skewed CPR [6]. However, in the TINRs, the $k_y = 0$ mode is strictly prohibited. Effectively, the small transverse size of the TINR generates a gap in the TSS spectrum, making the system more sensitive to disorder and rendering the CPR more sinusoidal. For $k_y \neq 0$, D depends on Z and is not necessarily 1; thus CPR is not necessarily highly skewed. Furthermore, in our SQUID-based measurement, we need to ensure that the current through the reference junction (part of our SQUID device) is sufficient to drive it to the normal state. Since I_c of the reference junction is on the order of 10 to 20 μA (compared to $I_c \sim 20$–200 nA in the TINRs), the electron temperature in the CPR measurement could be substantially larger compared to that in the V_{dc}–I_{dc} measurements (used to extract I_c). Additionally, our TINRs are very sensitive to temperature and show a strong asymmetry between their critical current I_c and return current I_r (see Fig. S3 and Supplemental Material for more details [37]) due to the Joule heating (caused by I_{dc}). Overall, the sensitivity to disorder for modes with $k_y \neq 0$ as well as the increased electron temperature due to the large I_c of the reference junction may result in sinusoidal CPR in our TINR-based JJs measured in the SQUID setup.

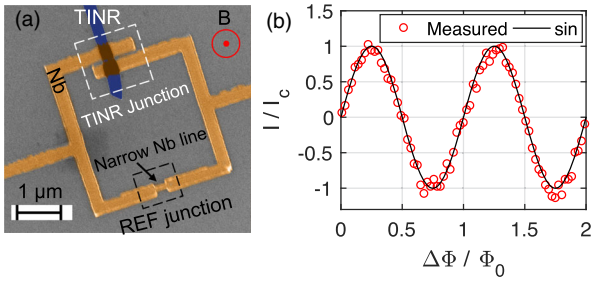

FIG. 3. (a) False-colored scanning electron microscope image of an asymmetric SQUID used to measure the current-phase relations (CPR) in our TINR-based JJs. (b) Normalized current I/I_c vs normalized flux $\Delta\Phi/\Phi_0$, where $\Phi_0 = h/2e$ is the flux quantum, at $V_g = 20$ V and $T = 20$ mK. As the absolute value of the flux inside the superconducting SQUID is unknown, the experimental curve is shifted along the horizontal axis for comparison with a sinusoidal function.

In this Letter, we present transport measurements of the JJs based on nanoribbons of the bulk-insulating topological insulators $BiSbTeSe_2$ with superconducting Nb contacts. We experimentally find an anomalous behavior in the T dependence of I_c in a variety of junctions with different T_c and V_g's. For all samples, I_c increases with decreasing temperature from T_c to an upturn temperature ($\sim 0.2T_c$), followed by an exponential increase with further decrease of the temperature. To understand our results, we introduce a phenomenological model based on the winding of the ABS around the circumference of the TINR. Our model relates the enhancement of I_c at low temperatures to the anomalously small energy scale of ABS in the long-junction limit. Furthermore, our measured CPR shows a sinusoidal behavior, consistent with the expectation for such long JJs under the experimental conditions. Our experimental observations indicate that our TINR junctions can be promising platforms for further exploration of topological superconductivity and

Majorana fermions predicted in TI-superconductor hybrid systems [4].

M. K. (Purdue), L. P. R., and Y. P. C. acknowledge support from National Science Foundation (NSF) under Grant No. DMR-1410942. M. K. (Purdue) and Y. P. C. also acknowledge partial support from NSF under Grant No. EFMA-1641101. L. P. R. and A. K. acknowledge partial support from the U.S. Department of Energy (DOE), Office of Basic Energy Sciences (BES) under Award No. DE-SC0008630 (L. P. R.) and Department of Defense Office of Naval Research Grant No. N000141410339 (A. K.). M. K. (UMD) acknowledges support by NSF DMR-1613029 and V. M. G. acknowledges support from the DOE, Office of BES (Award No. DE-SC0001911) and the Simons Foundation. The authors also acknowledge helpful discussions with Sergei Khlebnikov, Erhai Zhao, and Pouyan Ghaemi.

*mkayyalh@purdue.edu
†yongchen@purdue.edu

[1] M. Z. Hasan and C. L. Kane, Rev. Mod. Phys. **82**, 3045 (2010).
[2] X.-L. Qi and S.-C. Zhang, Rev. Mod. Phys. **83**, 1057 (2011).
[3] M. Z. Hasan and J. E. Moore, Annu. Rev. Condens. Matter Phys. **2**, 55 (2011).
[4] L. Fu and C. L. Kane, Phys. Rev. Lett. **100**, 096407 (2008).
[5] L. P. Gor'kov and E. I. Rashba, Phys. Rev. Lett. **87**, 037004 (2001).
[6] G. Tkachov and E. M. Hankiewicz, Phys. Rev. B **88**, 075401 (2013).
[7] X. Gong, M. Kargarian, A. Stern, D. Yue, H. Zhou, X. Jin, V. M. Galitski, V. M. Yakovenko, and J. Xia, Sci. Adv. **3**, e1602579 (2017).
[8] C. Beenakker, Annu. Rev. Condens. Matter Phys. **4**, 113 (2013).
[9] H.-J. Kwon, K. Sengupta, and V. M. Yakovenko, Eur. Phys. J. B **37**, 349 (2004).
[10] C. T. Olund and E. Zhao, Phys. Rev. B **86**, 214515 (2012).
[11] P. Burset, F. Keidel, Y. Tanaka, N. Nagaosa, and B. Trauzettel, Phys. Rev. B **90**, 085438 (2014).
[12] P. Ghaemi and V. P. Nair, Phys. Rev. Lett. **116**, 037001 (2016).
[13] G. Tkachov, Phys. Rev. Lett. **118**, 016802 (2017).
[14] B. Sacépé, J. B. Oostinga, J. Li, A. Ubaldini, N. J. Couto, E. Giannini, and A. F. Morpurgo, Nat. Commun. **2**, 575 (2011).
[15] D. Zhang, J. Wang, A. M. DaSilva, J. S. Lee, H. R. Gutierrez, M. H. W. Chan, J. Jain, and N. Samarth, Phys. Rev. B **84**, 165120 (2011).
[16] M. Veldhorst, M. Snelder, M. Hoek, T. Gang, V. K. Guduru, X. L. Wang, U. Zeitler, W. G. van der Wiel, A. A. Golubov, H. Hilgenkamp, and A. Brinkman, Nat. Mater. **11**, 417 (2012).
[17] J. R. Williams, A. J. Bestwick, P. Gallagher, S. S. Hong, Y. Cui, A. S. Bleich, J. G. Analytis, I. R. Fisher, and D. Goldhaber-Gordon, Phys. Rev. Lett. **109**, 056803 (2012).
[18] F. Qu, F. Yang, J. Shen, Y. Ding, J. Chen, Z. Ji, G. Liu, J. Fan, X. Jing, C. Yang, and L. Lu, Sci. Rep. **2**, 339 (2012).
[19] F. Yang, F. Qu, J. Shen, Y. Ding, J. Chen, Z. Ji, G. Liu, J. Fan, C. Yang, L. Fu, and L. Lu, Phys. Rev. B **86**, 134504 (2012).
[20] I. Sochnikov, A. J. Bestwick, J. R. Williams, T. M. Lippman, I. R. Fisher, D. Goldhaber-Gordon, J. R. Kirtley, and K. A. Moler, Nano Lett. **13**, 3086 (2013).
[21] J. B. Oostinga, L. Maier, P. Schüffelgen, D. Knott, C. Ames, C. Brüne, G. Tkachov, H. Buhmann, and L. W. Molenkamp, Phys. Rev. X **3**, 021007 (2013).
[22] S. Cho, B. Dellabetta, A. Yang, J. Schneeloch, Z. Xu, T. Valla, G. Gu, M. J. Gilbert, and N. Mason, Nat. Commun. **4**, 1689 (2013).
[23] C. Kurter, A. D. K. Finck, Y. S. Hor, and D. J. Van Harlingen, Nat. Commun. **6**, 7130 (2015).
[24] A. D. K. Finck, C. Kurter, Y. S. Hor, and D. J. Van Harlingen, Phys. Rev. X **4**, 041022 (2014).
[25] J. H. Lee, G.-H. Lee, J. Park, J. Lee, S.-G. Nam, Y.-S. Shin, J. S. Kim, and H.-J. Lee, Nano Lett. **14**, 5029 (2014).
[26] J. Wiedenmann, E. Bocquillon, R. S. Deacon, S. Hartinger, O. Herrmann, T. M. Klapwijk, L. Maier, C. Ames, C. Brüne, C. Gould, A. Oiwa, K. Ishibashi, S. Tarucha, H. Buhmann, and L. W. Molenkamp, Nat. Commun. **7**, 10303 (2016).
[27] M. P. Stehno, V. Orlyanchik, C. D. Nugroho, P. Ghaemi, M. Brahlek, N. Koirala, S. Oh, and D. J. Van Harlingen, Phys. Rev. B **93**, 035307 (2016).
[28] E. Bocquillon, R. S. Deacon, J. Wiedenmann, P. Leubner, T. M. Klapwijk, C. Brüne, K. Ishibashi, H. Buhmann, and L. W. Molenkamp, Nat. Nanotechnol. **12**, 137 (2017).
[29] L. A. Jauregui, M. Kayyalha, A. Kazakov, I. Miotkowski, L. P. Rokhinson, and Y. P. Chen, Appl. Phys. Lett. **112**, 093105 (2018).
[30] Y. Xu, I. Miotkowski, C. Liu, J. Tian, H. Nam, N. Alidoust, J. Hu, C.-K. Shih, M. Z. Hasan, and Y. P. Chen, Nat. Phys. **10**, 956 (2014).
[31] Y. Xu, I. Miotkowski, and Y. P. Chen, Nat. Commun. **7**, 11434 (2016).
[32] S. S. Hong, Y. Zhang, J. J. Cha, X.-L. Qi, and Y. Cui, Nano Lett. **14**, 2815 (2014).
[33] S. Cho, B. Dellabetta, R. Zhong, J. Schneeloch, T. Liu, G. Gu, M. J. Gilbert, and N. Mason, Nat. Commun. **6**, 7634 (2015).
[34] L. A. Jauregui, M. T. Pettes, L. P. Rokhinson, L. Shi, and Y. P. Chen, Nat. Nanotechnol. **11**, 345 (2016).
[35] A. Cook and M. Franz, Phys. Rev. B **84**, 201105 (2011).
[36] R. Ilan, J. H. Bardarson, H. S. Sim, and J. E. Moore, New J. Phys. **16**, 053007 (2014).
[37] See Supplemental Material at http://link.aps.org/supplemental/10.1103/PhysRevLett.122.047003 for further details regarding the sample parameters, temperature dependence of the critical current, and the measurement of the current-phase relation.
[38] P. Dubos, H. Courtois, B. Pannetier, F. K. Wilhelm, A. D. Zaikin, and G. Schon, Phys. Rev. B **63**, 064502 (2001).
[39] A. A. Golubov, M. Y. Kupriyanov, and E. Il'ichev, Rev. Mod. Phys. **76**, 411 (2004).

[40] L. Angers, F. Chiodi, G. Montambaux, M. Ferrier, S. Guéron, H. Bouchiat, and J. C. Cuevas, Phys. Rev. B **77**, 165408 (2008).
[41] C. T. Ke, I. V. Borzenets, A. W. Draelos, F. Amet, Y. Bomze, G. Jones, M. Craciun, S. Russo, M. Yamamoto, S. Tarucha *et al.*, Nano Lett. **16**, 4788 (2016).
[42] I. Borzenets, F. Amet, C. Ke, A. Draelos, M. Wei, A. Seredinski, K. Watanabe, T. Taniguchi, Y. Bomze, M. Yamamoto *et al.*, Phys. Rev. Lett. **117**, 237002 (2016).
[43] Y. Zhang and A. Vishwanath, Phys. Rev. Lett. **105**, 206601 (2010).
[44] J. H. Bardarson, P. W. Brouwer, and J. E. Moore, Phys. Rev. Lett. **105**, 156803 (2010).
[45] M. Tinkham, *Introduction to Superconductivity* (McGraw-Hill, New York, 1996), p. 454.
[46] J. Bardeen and J. L. Johnson, Phys. Rev. B **5**, 72 (1972).
[47] A. Svidzinsky, T. Antsygina, and E. N. Bratus, J. Low Temp. Phys. **10**, 131 (1973).
[48] P. F. Bagwell, Phys. Rev. B **46**, 12573 (1992).
[49] M. L. Della Rocca, M. Chauvin, B. Huard, H. Pothier, D. Esteve, and C. Urbina, Phys. Rev. Lett. **99**, 127005 (2007).
[50] M. Zgirski, L. Bretheau, Q. Le Masne, H. Pothier, D. Esteve, and C. Urbina, Phys. Rev. Lett. **106**, 257003 (2011).